Highly coherent mid-infrared supercontinuum generations in a strip titanium dioxide waveguide with three zero-dispersion wavelengths

JinYe Shen,[a] Jinhui Yuan,[a,b,*] Yujun Cheng,[a] Chao Mei,[b] Jintao Lai,[a] Xian Zhou,[b] Qiang Wu,[c,d] Binbin Yan,[a] Kuiru Wang,[a,*] Chongxiu Yu,[a] Xinzhu Sang[a]

[a]State Key Laboratory of Information Photonics and Optical Communications, Beijing University of Posts and Telecommunications, Beijing 100876, China

[b]Research Center for Convergence Networks and Ubiquitous Services, University of Science & Technology Beijing (USTB), Beijing 100083, China

[c]Department of Physics and Electrical Engineering, Northumbria University, Newcastle upon Tyne, NE1 8ST, United Kingdom

[d]Key Laboratory of Nondestructive Test (Ministry of Education), Nanchang Hangkong University, Nanchang 330063, China

Abstract. In this paper, a strip titanium dioxide (TiO_2) waveguide is designed for highly coherent mid-infrared (MIR) supercontinuum (SC) generation. For the designed TiO_2 waveguide, three zero-dispersion wavelengths (ZDWs) are obtained through adjusting the waveguide structure parameters. The three ZDWs are located at 1.53, 3.96, and 5.43 μm, respectively. The nonlinearity coefficient γ is calculated as 1.12 $W^{-1}m^{-1}$ at wavelength 3.1 μm. By optimizing the pump pulse parameters, the highly coherent MIR SCs are generated when the hyperbolic secant pump pulse with duration of 80 fs, peak power of 1 kW, and wavelength of 3.1 μm is launched into the TiO_2 waveguide and propagated after a 4.2 mm length. The obtained SC covers a wavelength range from 1.71 to 9.90 μm (more than 2.5 octaves). Our research results can find important applications in the MIR photonics and spectroscopy, biophotonics, optical precision measurement, etc.

Keywords: TiO_2 waveguide, Supercontinuum generation, Three zero-dispersion wavelengths.

***Corresponding Authors**, E-mail: yuanjinhui81@bupt.edu.cn; krwang@bupt.edu.cn

1 Introduction

Generation of the supercontinuum (SC) has attracted great research interests due to its extensive applications in the molecular spectroscopy, optical communication, biomedical science, etc [1-6]. Highly nonlinear optical materials are usually used as the media to generate the mid-infrared (MIR) SCs, such as chalcogenide glass fiber [7,8], fluoride and tellurite glass fibers [9-11], and so on. It is reported that the mid-infrared SC spanning from 1.4 to 13.3 μm was obtained in a soft-glass optical fiber by using the pump pulse with peak power of 2.29 MW and central wavelength of 6.3 μm [12]. In 2017, Han et al. fabricated a chalcogenide suspended-core optical

fiber and generated a SC with spectral width of 2-8 μm [13]. In the same year, Zhao et al. obtained the mid-infrared SC covering from 2.0 to 16 μm using a low-loss telluride single-mode optical fiber [14]. Compared with optical fibers, the optical waveguide size is smaller, the limiting ability of the light field is stronger, and thus it has unique advantages in the miniaturization and integration. Moreover, because the used optical materials such as chalcogenide glasses (As_2S_3, As_2Se_3) [15,16], group IV semiconductors (silicon, germanium, silicon nanocrystals) [17-19], and organics (PTS) [20] usually have high nonlinear refractive indices, the strong nonlinear interaction can occur in the nanoscale geometric size and millimeter waveguide length. In 2017, Yuan et al. proposed a suspended germanium-membrane ridge waveguide, in which the SC spanning from 1.96 to 12 μm was generated [21]. In 2021, Than Singh Saini et al. designed a tellurium-oxide coated silicon-nitride hybrid waveguide, where the SC extending from 0.88 to 5.22 μm was generated [22]. In 2022, Zhang et al. proposed a polarization-insensitive reverse-ridge AlGaAs waveguide, where for the quasi-TE and quasi-TM modes, the SCs extended from 2.17 to 8.53 μm and 2.23 to 8.61 μm, respectively [23]. At present, the manufacturing technology of the nonlinear waveguides is relatively mature. The MIR SC generations in these nonlinear waveguides have already been demonstrated.

TiO_2 has a wide transparent window from the visible to MIR spectral region (0.4-10 μm) [24] and a wide band gap of 3.4eV [25,26]. Its linear and nonlinear refractive indices are 2.3 times and 30 times that of silica, respectively [27,28]. The two-photon absorption after wavelength 800 nm can be ignored [29]. In addition, the TiO_2 waveguide has been fabricated with a propagation loss of ~5 dB/cm at the communication wavelengths [28]. Therefore, it can be a promising material for the integrated nonlinear photonics. Until now, some nonlinear optical effects in TiO_2 waveguides have already been studied, including spectral broadening [30],

Raman scattering [31,32], third-harmonic generation [33], and four-wave mixing [34]. However, there are few reports on the SC generation in the TiO_2 waveguide.

In this paper, we design a simple strip TiO_2 waveguide with three ZDWs. The three ZDWs are located at 1.53, 3.96, and 5.43 μm, respectively, and a low and flat dispersion profile is achieved in the considered wavelength range. The effects of the pump pulse and waveguide parameters on the SC generations are investigated. When the hyperbolic secant pump pulse with wavelength of 3.1 μm, peak power of 1000 W, and duration of 80fs is launched into the TiO_2 waveguide and propagated after a 4.2 mm length, the highly coherent MIR SC in the wavelength range of 1.71 to 9.90 μm (more than 2.5 octaves) is generated.

2 Theoretical model

The propagation dynamics of the SC generation in the TiO_2 waveguide can be modelled by the modified generalized nonlinear Schrodinger equation (GNLSE) as following [35]

$$\frac{\partial A(z,t)}{\partial z}+\frac{\alpha}{2}A(z,t)-\sum_{m\geq 2}\frac{t^{m+1}\beta_m(\omega)}{m!}\frac{\partial^m A(z,t)}{\partial t^m}=i\left(\gamma(\omega_0)+i\gamma_1(\omega_0)\frac{\partial}{\partial t}\right)\times\left[A(z,t)\int_0^\infty R(t')\left|A(z,t-t')\right|^2 dt'\right], \quad (1)$$

where $A(z,t)$ is the electrical field amplitude, α is the linear loss coefficient of the waveguide, $\beta_m(\omega)$ is the m-th order dispersion coefficient calculated from the Taylor expansion of the propagation constant, t is the retarded time, γ is the nonlinear coefficient, and γ_1 is the first-order derivative of γ. $\gamma(\omega)$ depends on the effective mode filed area A_{eff} and nonlinear refractive index n_2 ., which can be described as

$$\gamma=\frac{2\pi n_2}{\lambda A_{eff}}=\frac{2\pi}{\lambda}\frac{\iint n_2(x,y)\left|\overrightarrow{F(x,y)}\right|^4 dxdy}{\left(\iint\left|\overrightarrow{F(x,y)}\right|^2 dxdy\right)^2}, \quad (2)$$

$\overrightarrow{F(x,y)}$ represents the transverse distribution of the light field [36]. $n_2(x, y)$ is the nonlinear refractive index In this work, n_2 is taken as 2.3×10^{-17} m^2/W [24]. In general, the fabricated TiO_2

waveguides has a propagation loss of ~ 5 dB/cm at the telecommunication wavelengths [27]. Therefore, α could be taken as 5 dB/cm.

In addition, the third-order nonlinear effects and instantaneous are also considered, including the self-phase modulation, Raman scattering, and self-steeping. R(t) can be described as

$$R(t) = (1 - f_R)\delta(t) + f_R h_R(t), \tag{3}$$

where f_R is the fractional contribution of the Raman effect, and the Raman response function $h_R(t)$ has the following form

$$h_R(t) = \frac{\tau_1^2 + \tau_2^2}{\tau_1 \tau_2^2} \exp\left(-\frac{t}{\tau_2}\right) \sin\left(\frac{t}{\tau_1}\right), \tag{4}$$

where $\tau_1 = 37\times10^{-15}$ and $\tau_2 = 1.4\times10^{-12}$ are the inverses of the phonon oscillation frequency and bandwidth of the Raman gain spectrum, respectively [30].

The degree of the first-order coherence $g_{12}^{(1)}(\lambda)$ can be evaluated from the following formula

$$g_{12}^{(1)}(\lambda) = \frac{\left\langle E_1^*(\lambda) E_2(\lambda) \right\rangle}{\sqrt{\left\langle |E_1(\lambda)|^2 \right\rangle \left\langle |E_2(\lambda)|^2 \right\rangle}}, \tag{5}$$

where $E(\lambda)$ is the spectral amplitude of the SC, which can be obtained by the separate simulation of different input noises. The noise can be described as

$$n = \eta \hat{N} \exp(i 2\pi \hat{U}), \tag{6}$$

where η is the noise factor and describes the noise amplitude of the input pulse. $\hat{N}$ is a normal scattered random variable of average 0 and standard deviation 1. $\hat{U}$ is an evenly distributed random variable between 0 and 1. In this work, we perform 100 independent simulations and calculate the average of a pair of output fields.

3 Waveguide structure and characteristics

The structure of the TiO_2 waveguide is shown in Fig. 1(a), where the core and substrate materials of the waveguide are the titanium dioxide and silicon dioxide, respectively. And the outer surface of the waveguide is surrounded by air. From Fig. 1(a), the strip TiO_2 waveguide has a large refractive index contrast between the core and the substrate, which is conducive to the mode confinement in the core region of the waveguide. The width and height of the waveguide core are represented by W and H, respectively. When W and H are chosen as 6 and 0.75 μm respectively, the mode field distributions of the quasi-TE modes calculated at wavelengths 2, 4, and 6 μm are shown in Fig. 1(b). From Fig. 1(b), most of the mode field energies are confined in the waveguide.

The desired dispersion curve can be obtained by reasonably adjusting the geometric parameters W and H of the waveguide. The influences of W and H on the dispersion curves can be analyzed by the finite element method. Figs. 2(a) and 2(b) show the variations of the dispersion curves of the quasi TE mode with wavelength when W and H change, respectively. From Fig. 2(a), as H increases from 0.65 to 0.95 μm, the value of D gradually increases, and the ZDW number of the dispersion curve gradually decreases from three to one. From Fig. 2(b), as H increases from 5 to 8 μm, all the dispersion curves have three ZDWs, and the differences between them are not obvious. Therefore, in order to obtain the dispersion curve with three ZDWs, the geometric parameters of the strip TiO_2 waveguide is chosen as W = 6 μm and H = 0.75 μm. The optimized dispersion curve is shown in Fig. 3(a). From Fig. 3(a), the three ZDWs are located at 1.53, 3.96, and 5.43, respectively. The anomalous dispersion region lies in the wavelength range of 1.53 to 3.96 μm, and the normal dispersion region lies in the wavelength range of 3.96 to 5.43 μm. Fig. 3(b) shows the variations of the nonlinear coefficient γ and

effective mode field area A_{eff} with wavelength. From Fig. 3(b), as the wavelength increases, the values of γ and A_{eff} gradually decrease and increase, respectively. This is mainly because when the wavelength increases, the energy of the guided mode gradually leaks into the buffer layer and air. The calculated γ is 1.12 $W^{-1}m^{-1}$ at wavelength 3.1 μm. In addition, as shown in Table 1, the up to 12-th order dispersion coefficients of the quasi-TE mode at wavelength 3.1 μm are considered in the following simulation.

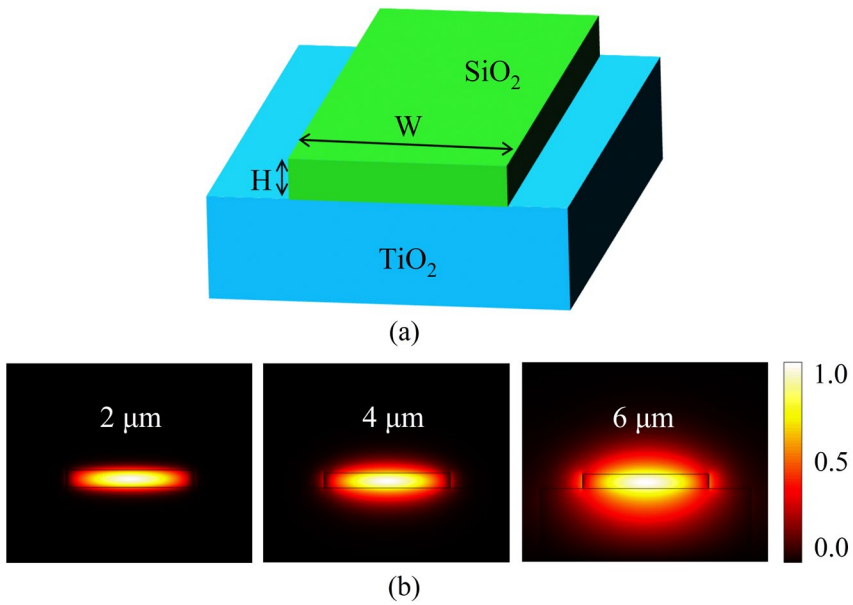

Fig. 1. (a) The structure of the proposed strip TiO_2 waveguide. (b) The mode filed distributions of the quasi-TE mode calculated at wavelengths 2, 4, and 6 μm, respectively, when W = 6 μm and H = 0.75 μm.

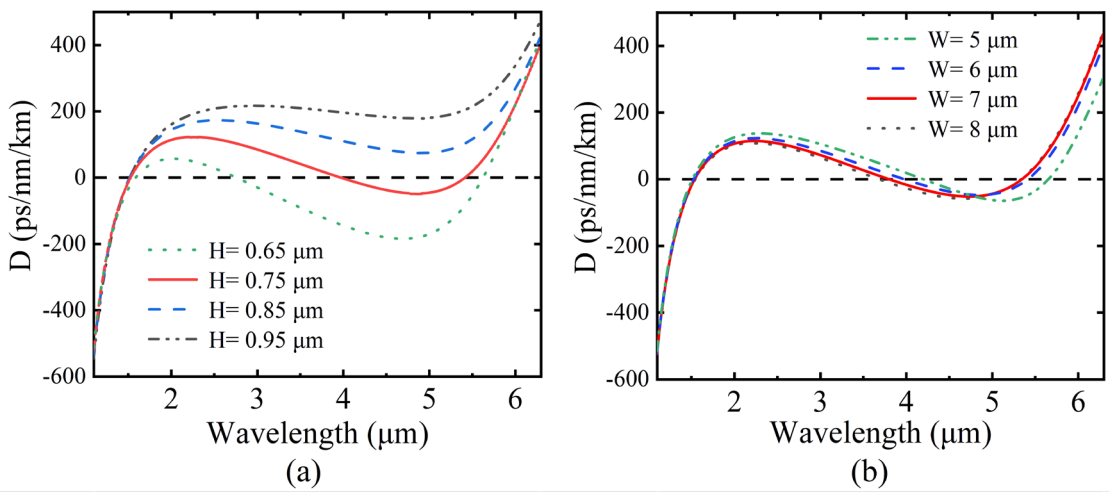

Fig. 2. The dispersion coefficient D of the quasi-TE mode calculated as a function of wavelength when (a) H and (b) W are changed, respectively.

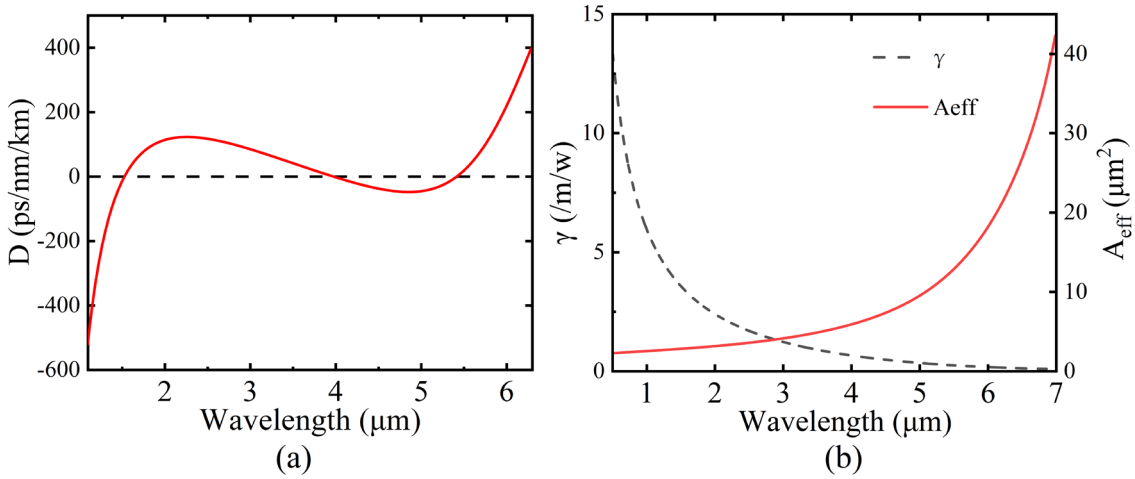

Fig. 3. (a) The dispersion curve of the quasi-TE mode calculated as functions of wavelength, along with the three ZDWs of 1.53, 3.96, and 5.43 μm, and (b) the effective mode field area A_{eff} and nonlinear coefficient γ calculated as functions of wavelength.

Table 1. The dispersion coefficient β_m calculated at wavelength 3.1 μm.

m	β_m
2	-0. 3639 ps^2/m
3	-3.0827×10^{-3} ps^3/m
4	2.5285×10^{-5} ps^4/m
5	1.01251×10^{-7} ps^5/m
6	-3.0473×10^{-9} ps^6/m
7	2.7468×10^{-11} ps^7/m
8	-1.5249×10^{-13} ps^8/m
9	5.8296×10^{-16} ps^9/m
10	-1.5621×10^{-18} ps^{10}/m
11	2.8411×10^{-21} ps^{11}/m
12	-3.1817×10^{-24}ps^{12}/m

4 Simulation results and discussion

The nonlinear dynamics of the SC generation in the proposed TiO_2 waveguide can be investigated by numerically solving Eq. (1) using the Runge-Kutta algorithm. The two-photon absorption and three photon absorption effects of the TiO_2 waveguide can be neglected within the considered spectral range [29]. In the following, we will investigate the influences of the pump pulse and waveguide parameters including the wavelength, peak power, pulse duration, and waveguide length on the SC generation. The spectral ranges of the SC discussed below are chosen at the power level of -40 dB.

The pump pulse is chosen as a hyperbolic secant pulse with peak power of 1000 W and duration of 80fs. When pumping at different wavelengths, the temporal and spectral profiles of the SC at the end of the 4.2-mm-long TiO_2 waveguide are shown in Figs. 4(a) and 4(b), respectively. From Figs. 4(a), when the pump wavelength is changed from 2.8 to 3.1 μm, the temporal pulse becomes narrower, and the irregular oscillation peaks begin to appear at the edges of the pulse when the pump wavelength is greater than 3 μm. From Fig. 4(b), with the increase of the pump wavelength, the spectral width at -40 dB bandwidth increases gradually. This is because the higher-order solitons are formed in the anomalous dispersion region, and both the higher-order dispersion and Raman effect will result in their fissions. At the same time, the self-phase modulation (SPM), cross-phase modulation (XPM), and dispersive-wave generation (DWG) will also occur, and they jointly broaden the optical spectrum. When the pump wavelength increases to 3.2 μm, the spectral width stops broadening and becomes narrower, which is mainly considered that the higher-order soliton fission process is remarkably suppressed by the second ZDW. Thus, the optimized pump wavelength is chosen as 3.1 μm. Fig. 4(c) shows the calculated first-order coherence of the SC. It can be seen from Fig. 4(c) the

coherence is maintained 1 in the considered wavelength range, which indicates that the SC has good coherence.

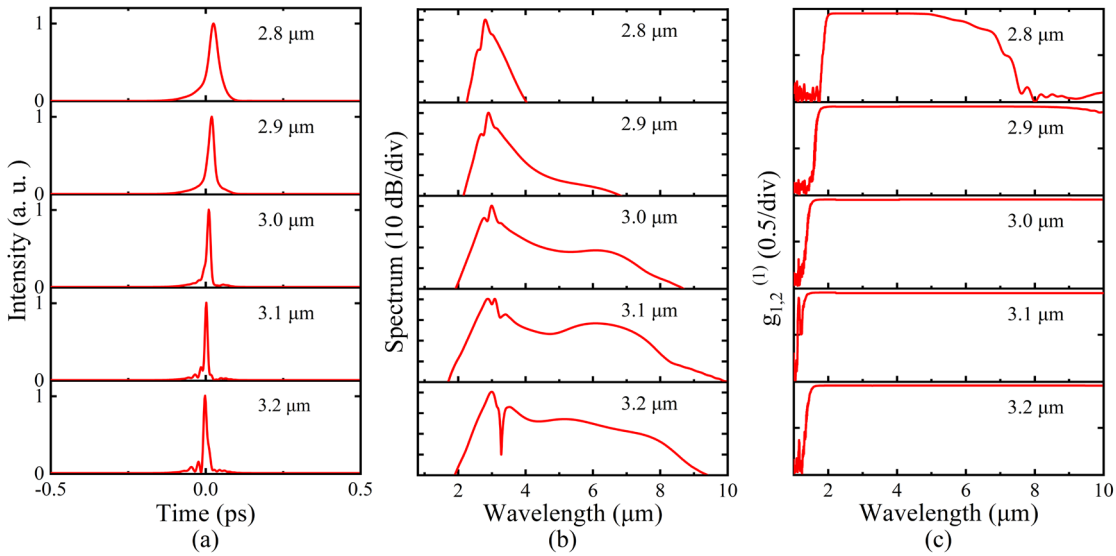

Fig. 4. (a), (b), and (c) show the temporal and spectral profiles and first-order coherence of the SCs generated in the TiO_2 waveguide when the wavelength of the pump pulse with peak power of 1000 W and duration of 80fs is changed from 2.8 to 3.2μm.

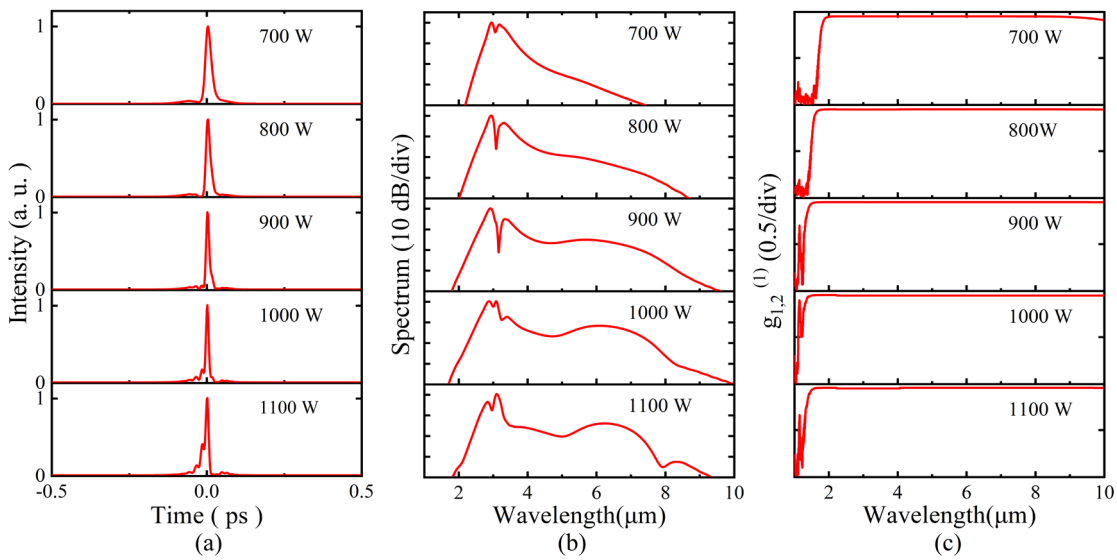

Fig. 5. (a), (b), and (c) show the temporal and spectral profiles and first-order coherence of the SC generated in the TiO_2 waveguide when the peak power of the pump pulse with wavelength of 3.1 μm and duration of 80 fs is changed from 700 to 1100 W.

When the peak power of the pump pulse with wavelength of 3.1 μm and duration of 80 fs is changed from 700 to 1100 W. the temporal and spectral profiles of the SC at the end of the

4.2-mm-long TiO_2 waveguide are shown in Figs. 5(a) and 5(b), respectively. From Fig. 5(a), as the peak power increases, the temporal pulse is basically unchanged, but the oscillation peaks begin to appear at the edges when the peak power is greater than 900 W. From Fig. 5(b), the spectral width increases as the peak power increases. This is because the high peak power will enhance a variety of nonlinear effects, resulting in a larger spectral width. In the process of the spectral broadening, the SPM, soliton dynamics, and XPM play important roles. However, when the peak power is saturated at 1100 W, the spectral broadening will stop. Thus, in order to obtain a wider SC, an appropriate peak power of 1000 W is chosen. The calculated first-order coherence of the SC is shown in Fig. 5(c). It can be seen from Fig. 5(c) that the generated SC has good coherence.

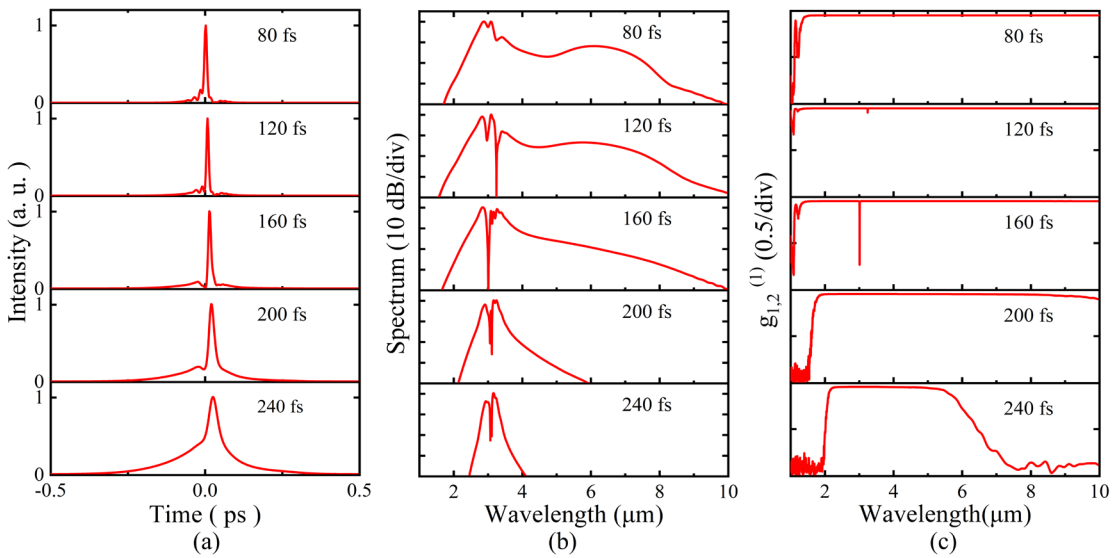

Fig. 6. (a), (b), and (c) show the temporal and spectral profiles and first-order coherence of the SC generated in the TiO_2 waveguide when the duration of the pump pulse with wavelength of 3.1 μm and peak power of 1000 W is changed from 80 to 250 fs.

Figs. 6(a) and 6(b) show the temporal and spectral profiles of the SC at the end of the 4.2-mm-long TiO_2 waveguide, respectively, when the duration of the pump pulse with wavelength of 3.1 μm and peak power of 1000 W is changed from 80 to 250 fs. From Fig. 6(a), as the pulse duration increases, the temporal pulse width gradually increases, and the oscillation

peaks emerging at the edges gradually disappear when the pulse duration is greater than 200 fs. From Fig. 6(b), the width of the optical spectra gradually decreases, along with multi-peak oscillations, which is due to the effect of the higher-order dispersion. In addition, for the larger pulse duration, the more pulse energy will be dispersed, resulting in the rapid reduction of the spectral width and the serious deterioration of the flatness. Thus, the pulse duration of 80 fs is chosen. Fig. 6(c) shows the calculated first-order coherence of the SC. From Fig. 6(c), the generated SC has good coherence.

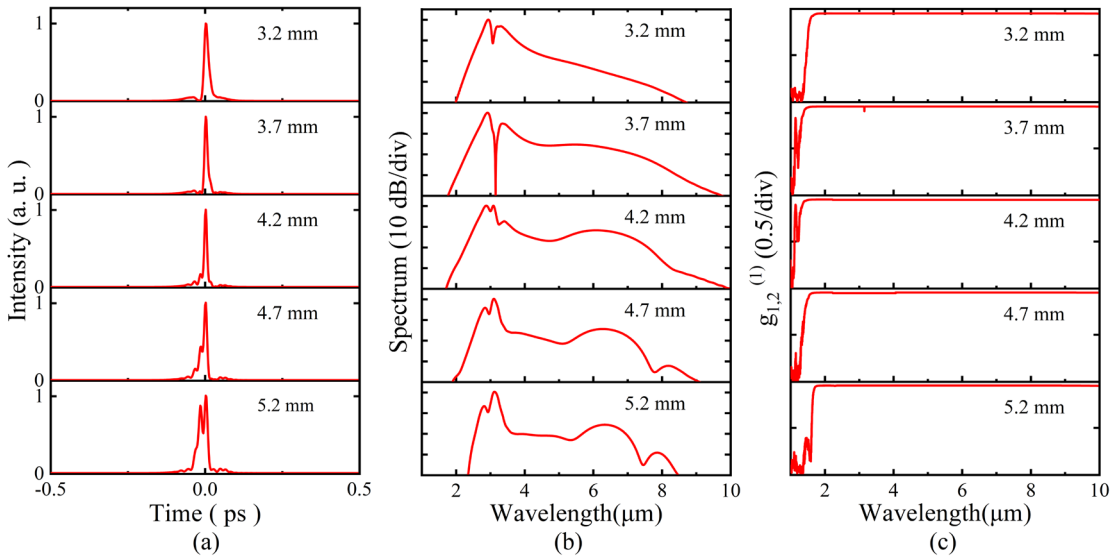

Fig. 7. (a), (b), and (c) show the temporal and spectral profiles and first-order coherence of the SC generated in the TiO_2 waveguide when the pump pulse with wavelength of 3.1 μm, peak power of 1000 W, and duration of 80 fs is used and the waveguide length is changed from 3.2 to 5.2 mm.

When the pump pulse with wavelength of 3.1 μm, peak power of 1000 W, and duration of 80 fs is used and the waveguide length is changed from 3.2 to 5.2 mm, the temporal and spectral profiles of the SC for different waveguide lengths are shown in Figs. 7(a) and 7(b), respectively. It can be observed from Fig. 7(a) that the temporal pulse becomes narrow first when the waveguide length increases to 4.2 mm, and then widens and occurs to split. From Fig. 7(b), when the waveguide length increases from 3.2 to 4.2 mm, the optical spectrum is gradually widened. This is resulted from the combined action of a series of nonlinear effects, including

SPM, soliton dynamics, XPM, and self-steepening. When the waveguide length exceeds 4.2 mm, most of the pulse energy is transferred to the pulse sidelobe due to the effect of the higher-order dispersion, so the optical spectrum gradually becomes narrower. At this time, the optimized waveguide length is 4.2 mm. Fig. 7(c) shows the calculated first-order coherence of the SC. From Fig. 6(c), the coherence of the generated SC is good.

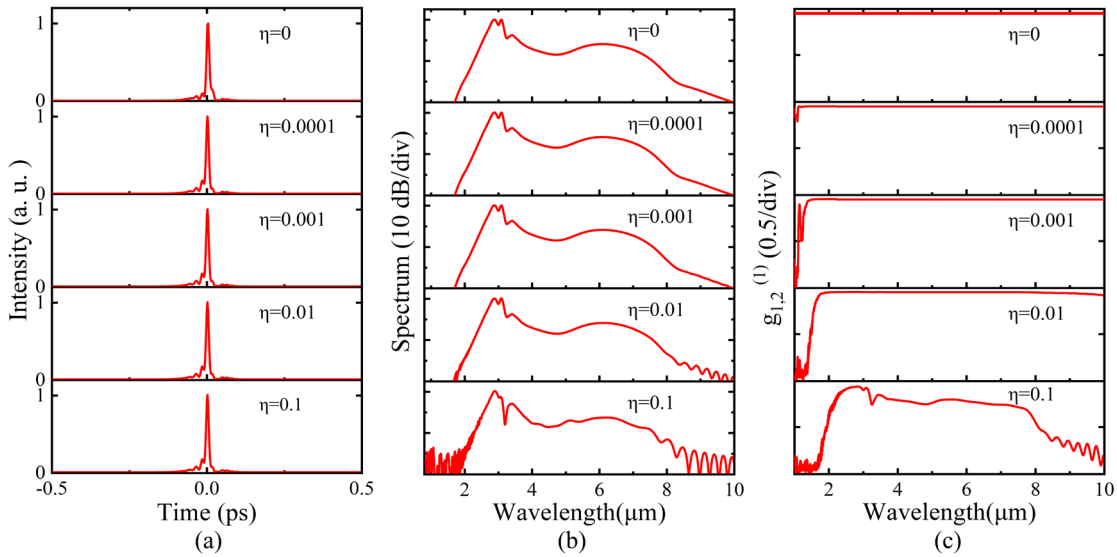

Fig. 8. (a), (b), and (c) show the temporal and spectral profiles and the first-order coherence of the SC generated in the TiO_2 waveguide when the pump pulse with wavelength of 3.1 μm, peak power of 1000 W, and duration of 80 fs is used, the waveguide length is chosen as 4.2 mm, and η is changed from 0 to 0.1.

When the pump pulse with wavelength of 3.1 μm, peak power of 1000 W, and duration of 80 fs is used and the noise figure η is changed from 0 to 0.1, the temporal and spectral profiles and the calculated first-order coherence of the SC at the end of the 4.2-mm-long TiO_2 waveguide are shown in Figs. 8(a), 8(b), and 8(c), respectively. From Fig. 8(a), as the noise coefficient η changes, the temporal pulse basically does not change. From Fig. 8(b), the flatness of the generated SC is better under a smaller η of 0.001. When η is larger than 0.01, the flatness of the SC begins to deteriorate. It can be seen from Fig. 8(c) that η has a certain impact on the coherence of the SC. When η is chosen as 0 or 0.001, the obtained SC has good coherence, while the coherence becomes worse for η=0.01 or 0.1. Thus, the value of η has a significant

impact on the coherence of the SC.

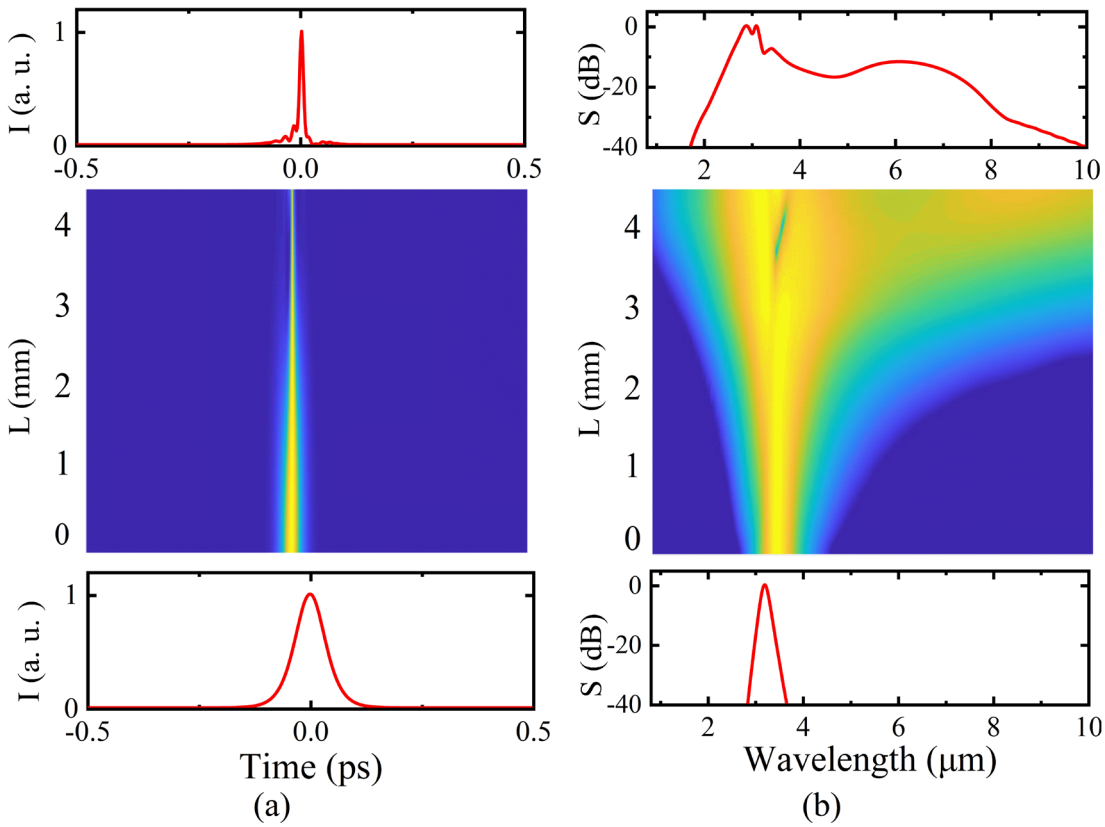

Fig. 9. (a) and (b) show the temporal and spectral evolutions of the pump pulse with wavelength of 3.1 μm, duration of 80 fs, and peak power of 1 kW in the 4.2-mm-long TiO_2 waveguide, respectively, the bottom and top figures showing the temporal and spectral profiles of the pump pulse at the input and output ends of the designed TiO_2 waveguide. *I* in (a) represents the intensity, *S* in (b) represents the spectrum.

Based on the above results, the hyperbolic secant pulse with wavelength of 3.1 μm, duration of 80 fs, and peak power of 1 kW is used as the pump source, and the noise coefficient η is chosen as 0.001. Figs. 9(a) and 9(b) show the temporal and spectral evolutions of the pump pulse in the 4.2-mm-long TiO_2 waveguide, respectively. At the same time, the temporal and spectral profiles of the pump pulse at the input and output ends of the waveguide are also given at the bottom and top of Figs. 9(a) and 9(b). From Fig. 9(a), the temporal pulse decreases with the increase of the propagation distance. After a propagation distance of 4.2 mm, some obvious oscillation peaks can be seen on the edge of the temporal pulse. From Fig. 9(b), as the propagation distance increases, the spectral width increases. When the propagation distance is

less than 2 mm, the optical spectrum is symmetrically widened under the action of the SPM effect. When the propagation distance is greater than 2 mm, the optical spectrum continues to extend towards the shorter and longer wavelength sides under the joint action of the soliton dynamics and XPM effect. Finally, after a propagation distance of 4.2mm, the SC generated at the output end of the waveguide spans from 1.89 to 9.98 μm, covering more than 2.5 octaves. Moreover, the MIR SC has good coherence.

5 Conclusion

In summary, we design a strip TiO_2 waveguide with the three ZDWs for generating the MIR SC. The effects of the pump pulse and waveguide parameters on the SC generation are investigated. When a hyperbolic secant pulse with wavelength of 3.1 μm, peak power of 1000 W, and duration of 80 fs is used as the pump source, the highly coherent MIR SC, which spans from 1.89 to 9.98 μm and covers more than 2.5 octaves, is generated at the output end of 4.2-mm-long waveguide. Our research results can find significant applications in the MIR photonics and spectroscopy, biophotonics, optical precision measurement, etc.

Acknowledgments

This work was supported by the National Natural Science Foundation of China (Grant No. 61875238).

References

1. A. Ruehl, M. J. Martin, et al., "Ultrabroadband coherent supercontinuum frequency comb," *J. Phys. Rev. A*. **84**(1), 011806 (2011).

2. S. V. Smirnov, J. D. Ania-Castanon, T. J. Ellingham, et al., "Optical spectral broadening and supercontinuum generation in telecom applications," *J. Opt. Fiber Technol.* **12**(2), 122-147 (2006).

3. J. Walther, M. Gaertner, P. Cimalla, et al., "Optical coherence tomography in biomedical research," *J. Anal. Bioanal. Chem.* **400**(9), 2721-2743 (2011).

4. A. Barkai, Y. Chetrit, O. Cohen, et al., "Integrated silicon photonics for optical networks," *J. Opt. Netw.* **6**(1), 25-47 (2007).

5. B. Jalali, S. Fathpour, "Silicon photonics," *J. Lightw. Technol.* **24**(12), 4600-4615 (2006).

6. P. Dumon, G. Priem, L. R. Nunes, et al., "Linear and nonlinear nanophotonic devices based on silicon-on-insulator wire waveguides," *J. Appl. Phys.* **45**(8S), 6589-6602 (2006).

7. G. Lenz, J. Zimmermann, T. Katsufuji, et al., "Large Kerr effect in bulk Se-based chalcogenide glasses," *J. Opt. lett.* **25**(4), 254-256 (2000).

8. J. M. Harbold, F. O. Ilday, F. W. Wise, et al., "Highly nonlinear As-S-Se glasses for alloptical switching," *J. IEEE Photon. Technol. Lett.* **14**(6), 822-824 (2002).

9. W. Yang, B. Zhang, G. Xue, et al., "Thirteen watt all-fiber mid-infrared supercontinuum generation in a single mode ZBLAN fiber pumped by a 2 μm MOPA system," *J. Opt. lett.* **39**(7), 1849-1852 (2014).

10. P. Domachuk, N. A. Wolchover, M. Cronin-Golomb, et al., "Over 4000 nm Bandwidth of Mid-IR Supercontinuum Generation in sub-centimeter Segments of Highly Nonlinear Tellurite PCFs," *J. Opt. Express.* **16**(10), 7161-7168 (2008).

11. O. Mouawad, J. Picot-Clémente, F. Amrani, et al., "Multioctave midinfrared supercontinuum generation in suspended-core chalcogenide fibers," *J. Opti. Lett.* **39**(9), 2684-2687 (2014).

12. S. S. Than, K. S. Ravindra, "Mid-infrared supercontinuum generation in soft-glass specialty optical fibers: A review," *Prog. Quantum. Electron.* **78**, 100342 (2021).

13. X. Han, C. You, S. Dai, et al., "Mid-infrared supercontinuum generation in a three-hole $Ge_{20}Sb_{15}Se_{65}$ chalcogenide suspended-core fiber," *J. Opt.Fiber Technol.* **34**, 74-79 (2017).
14. Z. M. Zhao, B. Wu, X. S. Wang, Z. H. Pan, Z. J. Liu, P. Q. Zhang, X. Shen, Q. H. Nie, S. X. Dai, R. P. Wang, "Mid-infrared supercontinuum covering 2.0–16 μm in a low-loss telluride single-mode fiber," *Laser Photon. Rev.* **11** (2), 1700005 (2017).
15. B. J. Eggleton, B. Luther-Davies, K. Richardson, "Chalcogenide photonics," *J. Nat. Photon.* **5**(3), 141-148 (2011).
16. B. Luther-Davies, "Flexible chalcogenide photonics," *J. Nat. Photon.* **8**(8), 591–593 (2014).
17. A. Martínez, J. Blasco, P. Sanchis, et al., "Ultrafast All-Optical Switching in a Silicon-NanocrystalBased Silicon Slot Waveguide at Telecom Wavelengths," *J. Nano. Letters.* 2010, **10**(4), 1506-1511 (2010).
18. L. Zhang, A. M. Agarwal, L. C. Kimerling, et al., "Nonlinear Group IV photonics based on silicon and germanium: from near-infrared to mid-infrared," *J. Nanophotonics.* **3**(4-5), 247-268 (2014).
19. Z. Kang, J. Yuan, X. Zhang, et al., "CMOS-compatible 2-bit optical spectral quantization scheme using a silicon-nanocrystal-based horizontal slot waveguide," *J. Sci. Rep.* **4**(1), 7177 (2014).
20. C. Koos, P. Vorreau, T. Vallaitis, et al., "All-optical high-speed signal processing with silicon–organic hybrid slot waveguides," *J. Nat. Photon.* **3**(4), 216-219 (2009).
21. J. H. Yuan, Z. Kang, F. Li, et al, "Mid-infrared octave-spanning supercontinuum and frequency comb generation in a suspended germanium-membrane ridge waveguide," *J. Lightwave Technol.* **35**, 2994–3002 (2017).
22. S. S. Than, V. R. Supradeepa, "Tellurium-oxide coated silicon-nitride hybrid waveguide for near-to-mid-IR supercontinuum generation: design and analysis," *J Mod Opt.* **1**(68), 29-36 (2021).

23. L. Zhang, J. Yuan, Y. Cheng, C. Mei, J. Lai, X. Zhou, Q. Wu, B. Yan, K. Wang, C. Yu, X. Sang, "Polarization-insensitive reverse-ridge AlGaAs waveguide for the mid-infrared supercontinuum generation," *Opt. Commun.* **502,** 127407 (2022).

24. M. Fu, Y. Zheng, G. Li, H. Hu, M. Pu, L. K. Oxenløwe, L. H. Frandsen, X. Li, X. Guan, "High-Q titanium dioxide micro-ring resonators for integrated nonlinear photonics," *Opt. Express.* **28**, 39084-39092 (2020)

25. J. D. B. Bradley, C. C. Evans, J. T. Choy, O. Reshef, P. B. Deotare, F. Parsy, K. C. Phillips, M. Lončar, E. Mazur, "Submicrometer-wide amorphous and polycrystalline anatase TiO2 waveguides for microphotonic devices," *Opt. Express.* **20**(21), 23821–23831 (2012).

26. C. C. Evans, C. Liu, J. Suntivich, "Low-loss titanium dioxide waveguides and resonators using a dielectric lift-off fabrication process," *Opt. Express.* **23**(9), 11160–11169 (2015).

27. C.C. Evans, K. Shtyrkova, J. D. B. Bradley, O. Reshef, E. Ippen, E. Mazur, "Spectral broadening in anatase titanium dioxide waveguides at telecommunication and near-visible wavelengths," *Opt. Express.* **21**, 18582–18591 (2013).

28. X. Guan, H. Hu, L. K. Oxenløwe, L. H. Frandsen, "Compact titanium dioxide waveguides with high nonlinearity at telecommunication wavelengths," *Opt. Express.* **26**, 1055–1063 (2018).

29. K. Hammani, L. Markey, M. Lamy, B. Kibler, J. Arocas, J. Fatome, A. Dereux, J. C. Weeber, C. Finot, "Octave Spanning Supercontinuum in Titanium Dioxide Waveguides," *Appl. Sci.* 2018, **8**(4), 543. https://doi.org/10.3390/app8040543.

30. C. C. Evans, K. Shtyrkova, J. D. B. Bradley, O. Reshef, E. Ippen, and E. Mazur, "Spectral broadening in anatase titanium dioxide waveguides at telecommunication and near-visible wavelengths," *Opt. Express.* **21**(15), 18582–18591 (2013).

31. J. Watanabe, "Stokes to Anti-Stokes Intensity Ratio in the Raman Scattering Spectra of Rutile TiO2——Raman Scattering Spectra," *J. Psy. Soc. Jpn.* **88**, 094706 (2019) 10.7566/JPSJ.88.094706

32. M. K. Ahmad, S. M Mokhtar, et al., “Raman investigation of rutile-phased TiO2 nanorods/nanoflowers with various reaction times using one step hydrothermal method,” *J Mater Sci: Mater Electron* **27**, 7920–7926 (2016). https://doi.org/10.1007/s10854-016-4783-z
33. C. C. Evans, K. Shtyrkova, O. Reshef, M. Moebius, J. D. Bradley, S. Griesse-Nascimento, E. Ippen, and E. Mazur, “Multimode phase-matched third-harmonic generation in sub-micrometer-wide anatase TiO2 waveguides,” *Opt. Express.* **23**(6), 7832–7841 (2015).
34. X. Guan, H. Hu, L. K. Oxenløwe, and L. H. Frandsen., “Compact titanium dioxide waveguides with high nonlinearity at telecommunication wavelengths,” *Opt. Express.* **26**(2), 1055–1063 (2018).
35. G. P. Agrawal., “Nonlinear fiber optics,” *Fifth ed.* (Academic Press, 2013).
36. M. T. Murphy, T. Udem, R. Holzwarth, et al., “High-precision wavelength calibration of astronomical spectrographs with laser frequency combs,” *Mon. Not. R. Astron. Soc.* **380**, 839–847 (2007).

Jinye Shen is currently a graduate student in the state Key Laboratory of Information Photonics and Optical Communication department at Beijing University of Posts and Telecommunications.

Jinhui Yuan received the Ph.D. degree in physical electronics from Beijing University of Posts and Telecommunications (BUPT), Beijing, China, in 2011. He is currently a Professor at the Department of computer and communication engineering, University of Science and Technology Beijing (USTB). His current research interests include photonic crystal fibers, silicon waveguide, and optical fiber devices. He is the Senior Members of the IEEE and OSA.

Yujun Cheng received the B.S. degree from Zhengzhou University, Zhengzhou, China, in 2016. In 2021, he received the Ph.D. degree from BUPT. His research interests include on-chip supercontinuum generation, frequency comb generation, pulse compression, and other nonlinear dynamics in optical devices and optical systems.

Chao Mei (Member, IEEE) received the B.S. degree in optical information science technology from Harbin Engineering University, Harbin, China, in 2013, and the Ph.D. degree in optical engineering from the Beijing University of Posts and Telecommunication, Beijing, China, in

2019. He is currently holding a postdoctoral position with the Max-Born Institute for Nonlinear Optics and Short Pulse Spectroscopy, Berlin, Germany, and cooperates with the University of Science and Technology Beijing, Beijing. His research interests are ultrafast optics, nonlinear optics, pulse shaping, nano-optics, and nonlinear dynamics in optical devices and optical systems.

Jintao Lai received the B.S. and M.S. degree from Beijing University of Posts and Telecommunications (BUPT), Beijing, China, in 2018 and 2021, respectively. His research interests include supercontinuum generation and SC-based frequency comb generation.

Xian Zhou (Member, IEEE) received the Ph.D. degree in the electromagnetic fifield and microwave technology from the Beijing University of Posts and Telecommunications (BUPT), Beijing, China, in 2011. She is currently a Professor with the Department of Computer and Communication Engineering, University of Science and Technology Beijing (USTB). She was selected as a Hong Kong Scholar at the Photonics Research Centre, Department of Electronics and Information Engineering, The Hong Kong Polytechnic University, in 2013. Her research interests are focused on high-speed optical communications, short-reach communications, and digital signal processing. She has published over 150 articles in academic journals and conferences.

Qiang Wu received the B.S. and Ph.D. degrees from Beijing Normal University and Beijing University of Posts and Telecommunications, Beijing, China, in 1996 and 2004, respectively. From 2004 to 2006, he worked as a Senior Research Associate with the City University of Hong Kong. From 2006 to 2008, he took up a Research Associate post at Heriot-Watt University, Edinburgh, U.K. From 2008 to 2014, he worked as a Stokes Lecturer with the Photonics Research Centre, Dublin Institute of Technology, Ireland. He is currently an Associate Professor/Reader with the Faculty of Engineering and Environment, Northumbria University, Newcastle Upon Tyne, U.K. His research interests include optical fifiber interferometers for novel fifiber optical couplers and sensors, nanofifiber, microsphere sensors for bio-chemical sensing, the design and fabrication of fifiber Bragg grating devices and their applications for sensing, nonlinear fifiber optics, surface plasmon resonant, and surface acoustic wave sensors. He has over 200 publications in the area of photonics and holds three invention patents. He is an

Editorial Board Member of Scientifific Reports, an Associate Editor for the IEEE SENSORS JOURNAL, and an Academic Editor for the Journal of Sensors.

Binbin Yan received the B.S. and M.S. degrees from Beijing University of Posts and Telecommunications (BUPT), Beijing, China, in 2003 and 2005, respectively. In 2009, she received the Ph.D. degree from BUPT. Now she is with the BUPT as an Associate Professor. Her research interests include photonic devices and fiber optic sensing.

Kuiru Wang received the B.S. and M.S. degrees from Beijing University of Posts and Telecommunications (BUPT), Beijing, China, in 1984 and 1990, respectively. In 2009, she received the Ph.D. degree from BUPT. Now she is with the BUPT as a Professor. Her current research interests include optical fiber communication and photonic devices.

Chongxiu Yu graduated from the Beijing University of Posts and Telecommunications (BUPT), Beijing, China, in 1969. Now she is with the BUPT as a Professor. Up to now she has published more than 300 papers. Her Research interests are the optical fiber communication, photonic switching, and optoelectronics technology and its applications. Prof. Yu is the Members of Chinese Institute of Communication, Committee of Fiber Optics and Integral Optics, and Chinese Optical Society.

Xinzhu Sang received the Ph.D. degree from Beijing University of Posts and Telecommunications (BUPT), Beijing, China, in 2005. Now he is with the BUPT as a professor. His current research interests include novel photonic devices, optical communication and optical interconnect. Prof. Sang is a senior Member of Chinese Institute of Communication, a committee of Holography and Optical Information Processing, Chinese Optical Society, and a member of OSA.

Captions List

Fig. 1. (a) The structure of the proposed strip TiO_2 waveguide. (b) The mode filed distributions of the quasi-TE mode calculated at wavelengths 2, 4, and 6 μm, respectively, when $W = 6$ μm and $H = 0.75$ μm.

Fig. 2. The dispersion coefficient D of the quasi-TE mode calculated as a function of wavelength when (a) H and (b) W are changed, respectively.

Fig. 3. (a) The dispersion curve of the quasi-TE mode calculated as functions of wavelength, along with the three ZDWs of 1.53, 3.96, and 5.43 μm, and (b) the effective mode field area A_{eff} and nonlinear coefficient γ calculated as functions of wavelength.

Fig. 4. (a), (b), and (c) show the temporal and spectral profiles and first-order coherence of the SCs generated in the TiO_2 waveguide when the wavelength of the pump pulse with peak power of 1000 W and duration of 80fs is changed from 2.8 to 3.2μm.

Fig. 5. (a), (b), and (c) show the temporal and spectral profiles and first-order coherence of the SC generated in the TiO_2 waveguide when the peak power of the pump pulse with wavelength of 3.1 μm and duration of 80 fs is changed from 700 to 1100 W.

Fig. 6. (a), (b), and (c) show the temporal and spectral profiles and first-order coherence of the SC generated in the TiO_2 waveguide when the duration of the pump pulse with wavelength of 3.1 μm and peak power of 1000 W is changed from 80 to 250 fs.

Fig. 7. (a), (b), and (c) show the temporal and spectral profiles and first-order coherence of the SC generated in the TiO_2 waveguide when the pump pulse with wavelength of 3.1 μm, peak power of 1000 W, and duration of 80 fs is used and the waveguide length is changed from 3.2 to 5.2 mm.

Fig. 8. (a), (b), and (c) show the temporal and spectral profiles and the first-order coherence of the SC generated in the TiO_2 waveguide when the pump pulse with wavelength of 3.1 μm, peak power of 1000 W, and duration of 80 fs is used, the waveguide length is chosen as 4.2 mm, and η is changed from 0 to 0.1.

Fig. 9. (a) and (b) show the temporal and spectral evolutions of the pump pulse with wavelength of 3.1 μm, duration of 80 fs, and peak power of 1 kW in the 4.2-mm-long TiO_2 waveguide, respectively, the bottom and top figures showing the temporal and spectral profiles of the pump pulse at the input and output ends of the designed TiO_2 waveguide. *I* in (a) represents the intensity, *S* in (b) represents the spectrum.

Table. 1. The dispersion coefficient β_m calculated at wavelength 3.1 μm.